

Oligosilanylated Antimony Compounds

Rainer Zitz,[†] Karl Gatterer,[‡] Crispin R. W. Reinhold,^{||} Thomas Müller,^{*,||} Judith Baumgartner,^{*,§} and Christoph Marschner^{*,†}

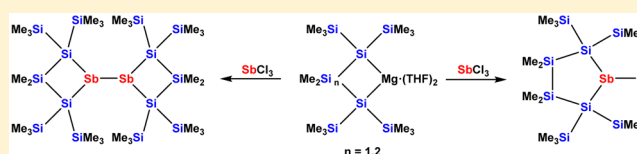
[†]Institut für Anorganische Chemie and [‡]Institut für Physikalische und Theoretische Chemie, Technische Universität Graz, Stremayrgasse 9, 8010 Graz, Austria

[§]Institut für Chemie, Karl Franzens Universität Graz, Stremayrgasse 9, 8010 Graz, Austria

^{||}Institut für Chemie, Carl von Ossietzky Universität Oldenburg, Carl von Ossietzky Str. 9-11, 26211 Oldenburg, Federal Republic of Germany

Supporting Information

ABSTRACT: By reactions of magnesium oligosilanides with SbCl_3 , a number of oligosilanylated antimony compounds were obtained. When oligosilanyl dianions were used, either the expected cyclic disilylated halostibine was obtained or alternatively the formation of a distibine was observed. Deliberate formation of the distibine from the disilylated halostibine was achieved by reductive coupling with C_8K . Computational studies of Sb–Sb bond energies, barriers of pyramidal inversion at Sb, and the conformational behavior of distibines provided insight for the understanding of the spectroscopic properties.



1. INTRODUCTION

Over the last 50 years, the chemistry of oligosilanes has experienced tremendous progress.^{1–4} In the course of this development, numerous examples of compounds substituted with heteroatoms were prepared and studied. The chemistry of group-15-substituted oligosilanes is dominated by aminosilanes and, to some lesser extent, phosphinosilanes. Examples of the heavier group 15 elements bearing oligosilanyl substituents, however, are quite scarce. For antimony in particular, only four compounds are known at all.^{5–7} These molecules were prepared by two different synthesis routes. Hassler and Seidl utilized reactions of alkali metal stibides with chlorosilanes to obtain dendrimeric⁵ or bicyclic⁶ compounds. Alternatively, Hopkins and co-workers utilized the reaction of $(\text{Me}_3\text{Si})_3\text{SiK}$ with SbCl_3 to obtain $[(\text{Me}_3\text{Si})_3\text{SiSb}]_4$.⁷ It should be noted that exactly the same type of chemistry was also reported with bismuth.^{5,6,8}

The oligosilanyl anion chemistry developed in our group over recent years⁹ has proven to be very useful for the synthesis of heteroatom-substituted oligosilanes.² With respect to group 15 compounds, however, this was limited to a single study demonstrating the availability of phosphacyclo- and bicyclosilanes.¹⁰ The current account intends to show how oligosilanyl anion chemistry can be used to establish some foundations of oligosilanylstibine chemistry.

2. RESULTS AND DISCUSSION

Our good experience of using oligosilanyl dianions for the synthesis of heterocyclosilanes^{10–16} encouraged us to attempt the synthesis of stibacyclosilanes by reaction of oligosilanyl dianions **1a** and **2a**¹² with antimony trichloride. However, the reactions were not successful because the major reaction

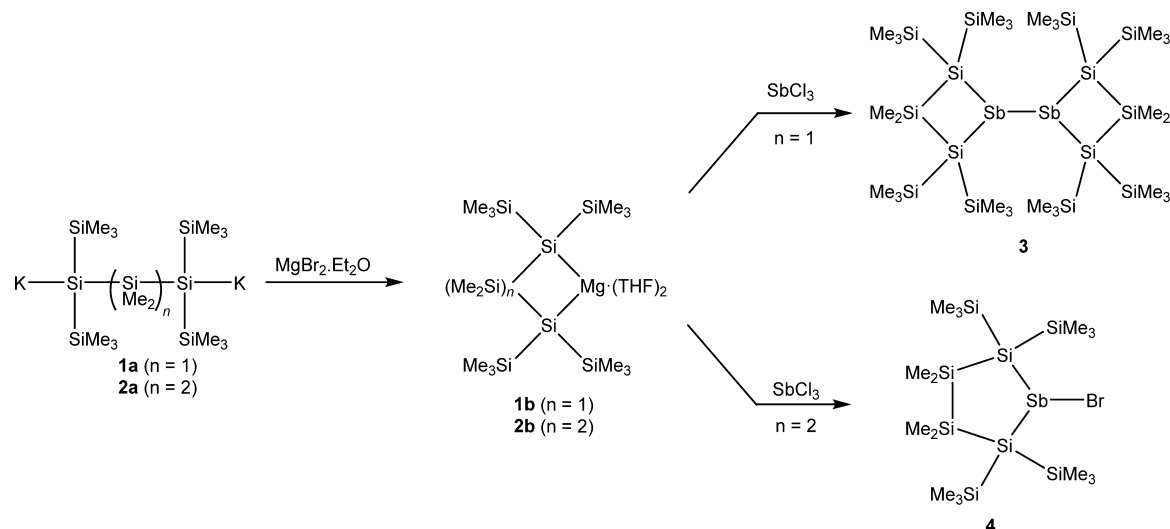
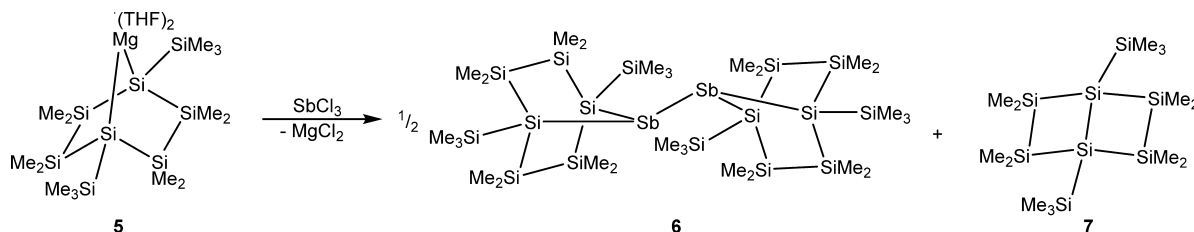
pathway in these cases was metal–halogen exchange leading to cyclosilane formation. To suppress this unwanted course of reaction, we switched to analogous magnesium silanediides **1b** and **2b**, which are readily available from the respective potassium silanediides by metathesis with magnesium bromide.¹³

Upon reaction of **1b** with SbCl_3 , formation of a 1-halo-1-stibacyclotetrasilane was expected. However, the respective distibine **3** was obtained instead in a modest yield of 28% (Scheme 1). The fact that **3** is formed instead of the expected halostibine can be explained with a metal–halogen exchange reaction of the initially formed halostibine with another equivalent of **1b**, leading to a magnesium stibide that can then react further with another halostibine to distibine **3**. Alternatively, the reduction of the halostibine to a radical followed by recombination to a distibine may also be a possibility, especially in light of the recent findings of stable antimony-centered radicals by Iwamoto and co-workers.¹⁷ In any case, the formation of distibines can only be imagined at the expense of some silanide.

It is important to note that using a 1:1 stoichiometry of the oligosilanyl dianion and SbCl_3 , a reaction sequence as proposed above limits the theoretically possible yield to 66% with respect to the used oligosilanyl dianion. The assumptions outlined are supported by the reaction of magnesium 1,4-cyclohexasilanediide **5**¹⁸ with SbCl_3 . Again a distibine (**6**) was formed, and in addition, the known bicyclo[2.2.0]hexasilane, **7**,¹⁸ was detected as the sole byproduct (Scheme 2). The latter is known to form from the respective dianion upon addition of 1,2-dibromo-

Received: October 27, 2014

Published: April 10, 2015

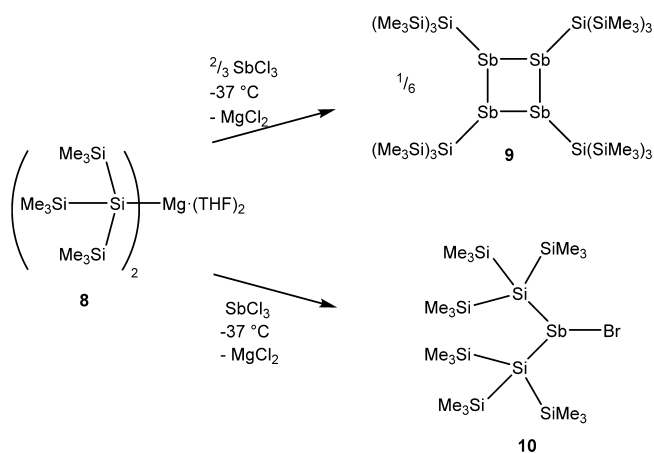
Scheme 1. Reactions of Magnesium Oligosilanyl Compounds **1b** and **2b** with SbCl_3 Scheme 2. Reaction of the Bicyclic Magnesium Oligosilanyl Compound **5** with SbCl_3 

ethane, which causes a potassium bromine exchange reaction as the first step followed by cyclization.¹⁸

The formation of distibines is likely related to what occurs in the formation of $[(\text{Me}_3\text{Si})_3\text{SiSb}]_4$ (**9**), as described by Hopkins and co-workers.⁷ This is supported by the large amount of $(\text{Me}_3\text{Si})_3\text{SiSi}(\text{SiMe}_3)_3$ formed as a byproduct in this reaction. To confirm this, we used an adapted protocol for the formation of $[(\text{Me}_3\text{Si})_3\text{SiSb}]_4$ (**9**), which utilizes $[(\text{Me}_3\text{Si})_3\text{Si}]_2\text{Mg}$ (**8**) instead of $(\text{Me}_3\text{Si})_3\text{SiK}$ and uses only $2/3$ equiv of SbCl_3 . Although the yield of the modified reaction conditions was still poor (13%) the purity of the obtained product allowed reassignment of the ^{29}Si NMR signals reported in the original study⁷ (*vide infra*) (Scheme 3). Repeating the reaction with an equimolar amount of SbCl_3 gave rise to the formation of bis[tris(trimethylsilyl)silyl]antimony bromide (**10**) (Scheme 3).

In an attempt to obtain a five-membered stibacyclosilane, SbCl_3 was reacted with magnesium tetrasilaniide **2b**. Comparison with the reaction of **1b** revealed a different outcome, and eventually the expected halostibine **4** was obtained in 70% yield. Compound **4** is, however, not the anticipated chlorostibine but rather a bromostibine, which was likely formed in a Finkelstein-type reaction with the magnesium bromide present in solution (Scheme 1). The bromostibyl unit is interesting as it allows further reactions at the antimony atom with nucleophiles and reducing agents.

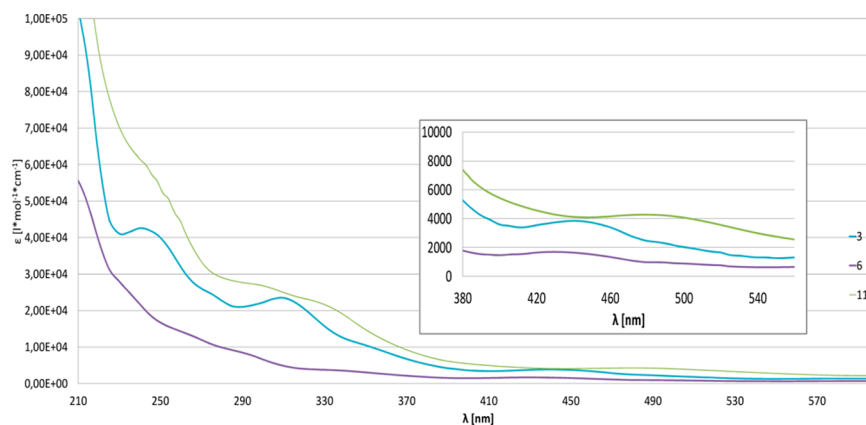
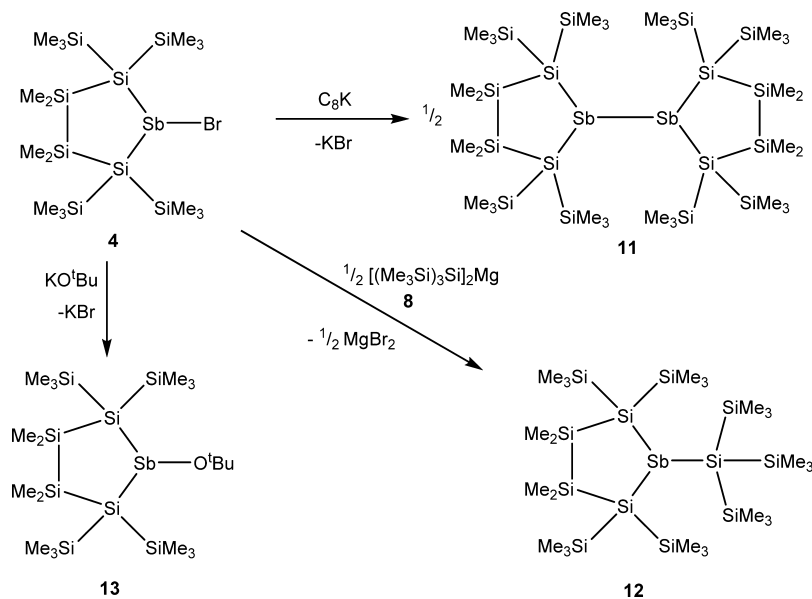
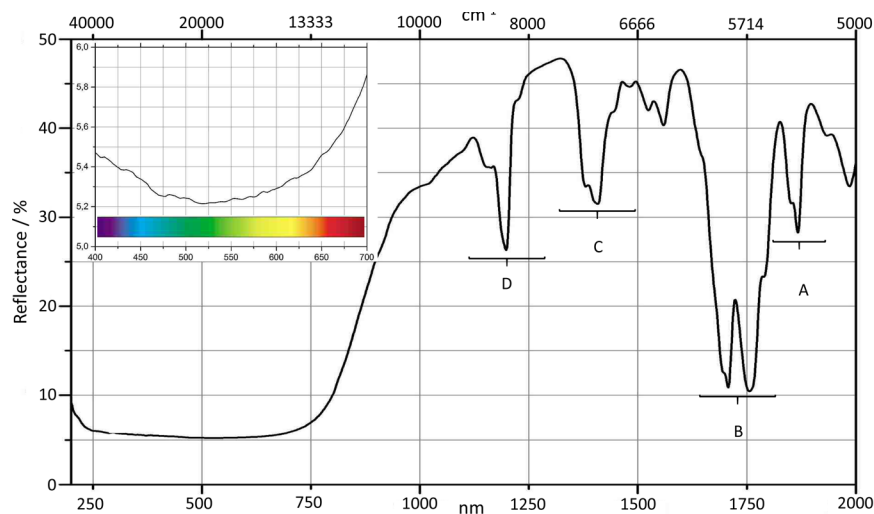
To obtain a distibine analogous to **3** and **6**, compound **4** was treated with potassium graphite (C_8K) to give rise to the formation of **11** (Scheme 4). When **4** was treated with potassium *tert*-butoxide the alkoxydistibine **13** was obtained in excellent yield (Scheme 4). Eventually reaction of **4** with half an

Scheme 3. Reactions of Bis[tris(trimethylsilyl)silyl]magnesium with SbCl_3 

equivalent of magnesium silanide **8** gave trisilylated stibine **12** (Scheme 4).

2.1. UV–Vis–NIR and IR Spectroscopy. A particularly interesting aspect of several distibines is their thermochromic behavior. Distibines of the type $[\text{R}_2\text{Sb}]_2$ ($\text{R} = \text{alkyl and aryl, EMe}_3$ ($\text{E} = \text{Si},^{19} \text{Ge},^{19} \text{Sn}^{20}$)) have therefore been studied intensively by UV–vis spectroscopy. Although the origin for the thermochromic property is not completely clear, one of the explanations involves intermolecular alignment in the solid state with rather short $\text{Sb}\cdots\text{Sb}$ distances (ca. 3.6–3.9 Å).²¹ This goes along with a change from red color for the solid phase to yellow for phases in solution. The low-energy bands of $[(\text{Me}_3\text{Si})_2\text{Sb}]_2$ ($\lambda_{\text{solid}} = 530 \text{ nm}$, $\lambda_{\text{soln}} = 430 \text{ nm}$),¹⁹

Scheme 4. Reductive Coupling, Silylation, and Alkoxylation Reactions of Bromostibine 4

Figure 1. UV-vis spectra of distibines **3**, **6**, and **11** in pentane.Figure 2. Diffuse reflectance spectrum of solid crystalline compound **11**. Inset: Extended scale view of the visible range.

$[(\text{Me}_3\text{Ge})_2\text{Sb}]_2$ ($\lambda_{\text{solid}} = 520 \text{ nm}$, $\lambda_{\text{solv}} = 400 \text{ nm}$),¹⁹ and $[(\text{Me}_3\text{Sn})_2\text{Sb}]_2$ ($\lambda_{\text{solid}} = 510 \text{ nm}$, $\lambda_{\text{solv}} = 360 \text{ nm}$),²⁰ are strongly blueshifted.¹⁹

Silylated distibines **3**, **6**, and **11** in this paper are also red-, orange-, or purple-colored solids; however, upon dissolving them they maintain their color. Although the solution low-

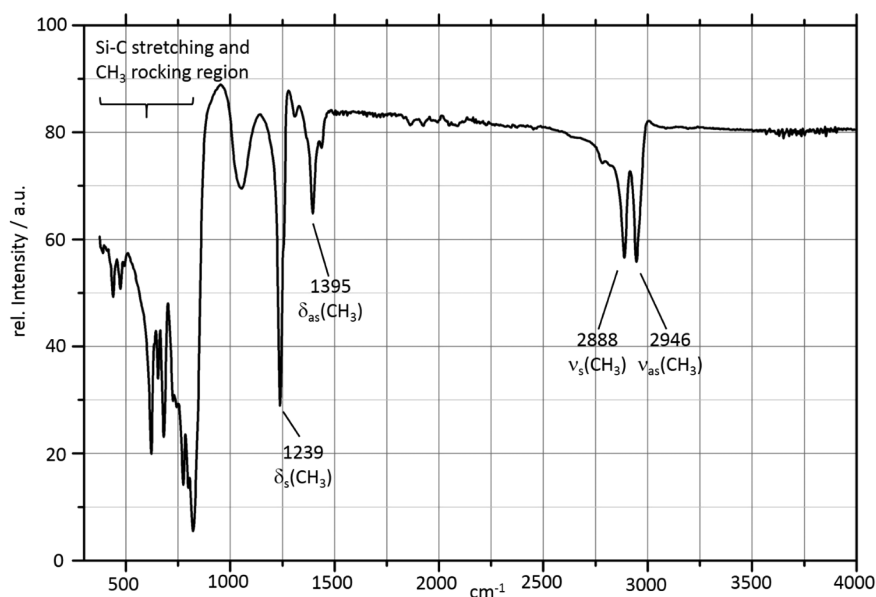


Figure 3. IR spectrum of solid crystalline compound **11**.

Table 1. NMR Spectroscopic Data of Oligosilanylstibyl Compounds^a

compound	¹ H (SiMe ₃)	¹ H (SiMe ₂)	¹³ C (SiMe ₃)	¹³ C (SiMe ₂)	²⁹ Si (SiMe ₃)	²⁹ Si (SiMe ₂)	²⁹ Si (Si _q)
3	0.45/0.41	0.56/0.52	4.6/2.5	6.4/5.1	-5.0/-8.7	-11.3	-102.1
4	0.42/0.21	0.42/0.26	3.8/2.6	-1.3	0.0/-7.5	-13.7	-98.1
6	0.46	0.51/0.36/0.31	3.8	0.1/-0.2/-1.58/-1.64	-4.7	-26.3/-32.9	-92.8
9	0.44	n.a.	4.3	n.a.	-6.1	n.a.	-114.5
10	0.34	n.a.	n.d.	n.a.	-5.0	n.a.	-95.7
11	0.43	0.37	4.3	-1.4	-6.5	-22.3	-112.1
12	0.38 (36H)/0.37 (27H)	0.40	3.6 (2 signals)	-1.5	-7.2/-8.3	-23.3	-110.8/-117.5
13	0.41/0.33	0.44/0.24	3.6/2.6	-1.2/-1.4	-3.4/-7.9	-17.8	-104.6

^aChemical shifts in ppm in reference to TMS.

energy bands of **3** and **6** are close to that of [(Me₃Si)₂Sb]₂, they are very broad (Figure 1). The red distibine, **11**, shows a distinctly different UV behavior with the low-energy band shifted to 478 nm. This is likely caused by the unusual conformational properties of **11** (*vide supra*).

For compound **11**, a diffuse reflectance spectrum in the UV–vis–NIR range was obtained (Figure 2).

Quite similar to the solid state spectra of (Me₃Si)₂SbSb(SiMe₃)₂,¹⁹ (Me₃Ge)₂SbSb(GeMe₃)₂,¹⁹ and (Me₃Sn)₂SbSb(SnMe₃)₂,²⁰ the spectrum of **11** is dominated by a broad unstructured absorption band in the visible range. In addition, a series of combinations and overtones of molecular vibrations is visible in the NIR part of the spectrum. The broad band accounts for the dark-purple color of **11** in that it shows slightly higher reflectance in the red and blue regions (see inset of Figure 2). To assign the bands in the NIR region, an infrared spectrum of the solid compound was recorded, which is shown in Figure 3.

A tentative assignment of the observed bands in the IR spectrum according to the literature²² is given in Figure 3. Using the experimentally found vibrational frequencies (in cm⁻¹) of compound **11**, a crude assignment of the four groups of bands (A–D) in Figure 2 in the NIR is possible. Region A (ca. 5250–5470 cm⁻¹) contains the second overtone of combinations of the bending vibrations δ_{as}(CH₃) and δ_s(CH₃), region B (ca. 5480–6060 cm⁻¹) contains the second overtone of combinations of the stretching vibrations ν_s(CH₃)

and ν_{as}(CH₃), region C (ca. 6840–7400 cm⁻¹) is a combination of the two stretching vibrations and one bending vibration, and region D (ca. 8250–8700 cm⁻¹) corresponds combinations of the second overtone of a stretching vibration with one of the bending vibrations.

2.2. NMR Spectroscopy. Because antimony does not have stable-spin 1/2 isotopes, NMR spectroscopic characterization of the obtained compounds has to concentrate on ¹H, ¹³C, and in particular on ²⁹Si NMR spectra (Table 1). ¹H, ¹³C, and ²⁹Si NMR spectra of **3** exhibit a molecular symmetry that is consistent with configurational stability of the antimony atom. Accordingly, side differentiation of the stibacyclotetrasilane is observed. The spectra of distibine **3** also reveal some influence of the antimony atom on the chemical shifts of the molecule. Interestingly, it is neither the neighboring silicon atoms nor the trimethylsilyl groups attached to those that is most affected but rather the SiMe₂ group. Comparison of **3** with 1,1,3,3-tetrakis(trimethylsilyl)tetramethylcyclotetrasilane²³ shows that ¹H and ¹³C shifts of the methyl groups are within the expected range. The same is true for the ²⁹Si shift of trimethylsilyl groups and the quaternary silicon atom. The latter displays the typical downfield shift characteristic for cyclotetrasilanes. The ²⁹Si NMR resonance of the SiMe₂ group is unexpected because its value of -11.3 ppm is considerably downfield to the -25.5 ppm found for 1,1,3,3-tetrakis(trimethylsilyl)tetramethylcyclotetrasilane.²³ If, however, the SiMe₂ shift of **3** is compared to 1,1,2,2-tetrakis(trimethylsilyl)tetramethylcyclotetrasilane,²⁴

then a rather similar value of -8.6 ppm was observed. Assessment of distibine **6** consisting of the two bicyclic [2.2.1] units shows again configurational stability of the antimony atoms. Therefore, four different signals for the SiMe_2 methyl groups are observed in the respective ^1H and ^{13}C spectra. The ^{29}Si NMR resonances for the SiMe_2 groups are at -26.3 and -32.9 ppm in an area close to the -31.7 ppm detected for 1,4-bis(trimethylsilyl)decamethylbicyclo[2.2.1]heptasilane.¹⁸

In contrast to the spectra of distibines **3** and **6**, the molecular symmetry of the third distibine, **11**, exhibits no configurational stability at antimony. Only one type of SiMe_3 and SiMe_2 groups are present, and additionally, the methyl groups of the SiMe_2 units are magnetically equivalent. An alternative explanation for this magnetic equivalence would be a rotation around the Sb–Sb bond of **11**. As pointed out below, this process is, however, energetically not feasible. All chemical shifts of **11** are in the expected ranges.

The spectra of the precursor to **11**, bromostibine **4**, show two different trimethylsilyl resonances in the ^1H , ^{13}C , and ^{29}Si spectra, indicating that the antimony atom exhibits configurational stability. As a consequence of this, two different resonances for the methyl groups of the SiMe_2 unit are also expected. In the ^1H NMR spectrum, one of these SiMe_2 signals overlaps with that of a SiMe_3 resonance at $\delta = 0.42$ ppm. In the ^{13}C spectrum, however, the two SiMe_2 signals exhibit the same chemical shift, as confirmed by 2D ^1H – ^{13}C correlation spectroscopy (gHSQC).

The structurally similar alkoxydistibine, **13**, which also features a configurationally stable antimony atom, shows all the required signals in expected ranges. Tris(trimethylsilyl)silylated stibacyclopentasilane **12** does not display side-differentiation of the ring. One may conclude that the reason for this is the steric bulk of the tris(trimethylsilyl)silyl group, but the effect is most likely electronic in nature because a trimethylsilylated stibacyclopentasilane (**16**) is also configurationally unstable.²⁵ All chemical shifts of **12** are within the expected ranges (Table 1). The NMR spectra of cyclotetradistibine **9** are completely as expected. The only reason to mention these spectra at all is that in the original report on the synthesis of this compound⁷ a much more complicated spectroscopic picture was described that was probably caused by the presence of some oligosilane side products.

2.3. Crystal Structure Analysis. The structures of compounds **3**, **4**, **6**, **9**, and **11**–**13** in this study were characterized by single-crystal X-ray diffraction (Tables S1 and S2). A compilation of the obtained structural data is given in Table 2. Containing Sb–Sb bonds, compound **9** and distibines **3**, **6**, and **11** are likely the most interesting compounds from a structural point of view. Intramolecular Sb–Sb distances of structurally characterized distibines as found in the Cambridge Crystallographic Database²⁶ comprise a range from 2.827 to 2.883 Å²⁶ with $[(\text{Me}_3\text{Sn})_2\text{Sb}]_2$ ²⁰ featuring the longest bond. In comparison to the already known data, the Sb–Sb bond distances of **3** (Figure 3), **6** (Figure 5), **9** (Figure 6), and **11** (Figure 7) are at the upper end of the expected range (2.85–2.88 Å). The Si–Sb distances of all compounds are a bit more diverse, ranging from 2.59 to 2.65 Å. This is clearly longer than the mean value of 2.56 Å obtained from a search in the Cambridge Crystallographic Database²⁶ and also the 2.60 Å of $[(\text{Me}_3\text{Si})_2\text{Sb}]_2$.²⁷ Nevertheless, considering the bulkiness of the oligosilanyl substituents, this is not surprising. In addition, the Sb–Br and Sb–O bond lengths of 2.55 and 2.01 Å, respectively, are completely within

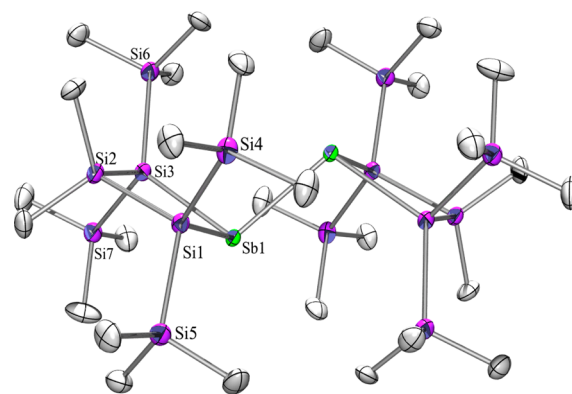


Figure 4. Molecular structure of **3** (thermal ellipsoid plot drawn at the 30% probability level). All hydrogen atoms are omitted for clarity. Bond lengths given in angstroms, angles in degrees. Sb(1)–Si(1) 2.628(2), Sb(1)–Si(3) 2.657(3), Sb(1)–Sb(1a) 2.8779(13), Si(2)–C(1) 1.890(8), Si(2)–Si(1) 2.354(3), Si(2)–Si(3) 2.365(3), Si(1)–Sb(1)–Si(3) 80.48(7), Si(1)–Sb(1)–Sb(1a) 103.10(6), Si(3)–Sb(1)–Sb(1a) 107.65(6).

the values expected for compounds with tricoordinate antimony atoms.²⁶

The structures of distibines **3** (Figure 4), **6** (Figure 6), and **11** (Figure 8) are surprisingly different. Although no extraordinary differences with respect to bond distances can be observed, the conformational situations of the three compounds are quite diverse. Distibine **3** presents itself as a molecule with an inversion center in the middle of the Sb–Sb bond. The two four-membered rings are parallel, and the angle of the Sb–Sb bond crossing the plane Si1–Sb–Si3 is $69.40(9)^\circ$, the largest of all three compounds. A comparison of structurally characterized distibines reveals the expected strong preference for a conformation where the two Sb-lone pairs are in trans position. This conformation is found perfectly for **3**, and it is also present in a slightly distorted form in **6**. Although the quality of the structure of distibine **11** is not as good as the ones of the compounds **3** and **6**, the difference in conformational behavior is nevertheless clearly visible. The Si–Sb–Si bond angle of the five-membered ring is considerably larger (approximately 99°) than those for **3** (80.5°) and **6** (approximately 85°), which brings the trimethylsilyl groups attached to the neighboring silicon atoms closer together. To avoid steric interaction, the angle of the Sb–Sb bond crossing the Si–Sb–Si plane is diminished to 50° , and in addition, the two rings are twisted along the Sb–Sb bond. A similar conformation was also observed for a recently reported tetraalkyl distibine that is in equilibrium with stibinyl radicals.¹⁷ It is likely that the particular conformation of **11** facilitates the inversion process of the antimony atom that was observed in the NMR spectra. This is in agreement with the fact that the Sb atoms of **3** and **6** are highly pyramidalized as indicated by the sums of bond angles around Sb of approximately 291° (Table 2). To minimize steric interaction, the degree of pyramidalization of Sb in distibine **11** is much less, displaying angle sums of 322 – 324° . It seems also likely that the strained distibine conformation is responsible for the fact that bromostibine is formed at all and also for the distinctly different UV–vis absorption behavior of **11** compared to that of **3** and **6**. Compared to the short intermolecular Sb⋯Sb distances²¹ found for the simpler distibines on the type $(\text{Me}_3\text{E})_2\text{SbSb}$

Table 2. Compilation of Structural Data Derived by Single Crystal XRD Analysis

compound	$d_{\text{Sb-X}}$ (Å)	$d_{\text{Si-Sb}}$ (Å)	$d_{\text{Si-SiMe}_3}$ (Å)	$d_{\text{Si-SiMe}_2}$ (Å)	\angle_{SiSbSi} (deg)	$\Sigma\angle_{\text{Sb}}$ (deg)	\angle_{SbSbX} (deg)	\angle_{SiSbSiSi} (deg)
3 (X = Sb)	2.8779(13)	2.628(3), 2.657(2)	2.341(4)– 2.360(4)	2.353(3), 2.365(4)	80.48(7)	291.21(5)	103.10(6), 107.65(6)	180/180
4 (X = Br)	2.5584(14)	2.618(2)	2.3538(19), 2.350(2)	2.3536(18)	98.67(6)	297.98(5)	110.22(6)	n.a.
6 (X = Sb)	2.8646(8)	2.6165(17)– 2.636(2)	2.352(2)– 2.362(2)	2.335(3)– 2.373(3)	84.56(6), 85.34(6)	289.97(5), 291.19(5)	90.42(4)/115.43(4), 91.05(4)/114.36(4)	160.70(6)/160.17(6)
9 (X = Sb)	2.853(1)– 2.8699(9)	2.616(2)– 2.631(2)	2.336(4)– 2.369(2)	n.a.	n.a.	283.60(4), 287.37(4), 294.83(4), 299.99(4)	96.61(4)–106.70(4)	n.a.
11 (X = Sb)	2.879(2), 2.875(1)	2.609(4)– 2.637(4)	2.348(5)– 2.388(5)	2.347(6)– 2.374(5)	98.81(10)– 99.18(10)	324.2(1), 322.2(1), 323.5(1), 322.2(1)	95.41(8)/127.65(8), 100.40(8)/124.62(8)	125.6(1)/122.7(1), 123.8(1)/121.8(1)
12 (X = Si)	2.6292(17)	2.6226(15), 2.6377(15)	2.354(2)– 2.375(2)	2.352(2), 2.358(2)	100.43(5)	329.61(5)	111.58(5)/117.60(5)	n.a.
13 (X = O)	2.0097(17)	2.5943(8), 2.6097(10)	2.346(1)– 2.349(1)	2.348(1), 2.352(1)	97.76(2)	296.12(5)	96.80(5)/101.56(5)	n.a.

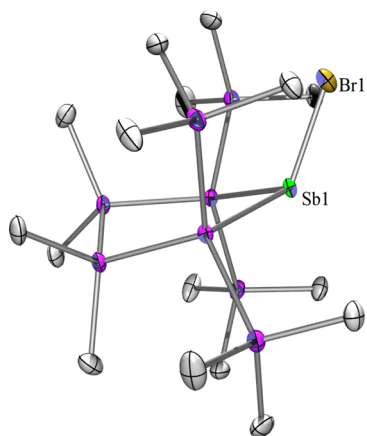


Figure 5. Molecular structure of **4** (thermal ellipsoid plot drawn at the 30% probability level). All hydrogen atoms are omitted for clarity. Bond lengths given in angstroms, angles in degrees. Sb(1)–Br(1A) 2.5548(14), Sb(1)–Si(1) 2.618(2), Si(1)–Si(2) 2.3536(18), Si(1)–Si(3) 2.3538(19), Si(2)–C(1) 1.885(5), Br(1A)–Sb(1)–Si(1A) 98.26(7), Si(1A)–Sb(1)–Si(1) 98.67(6).

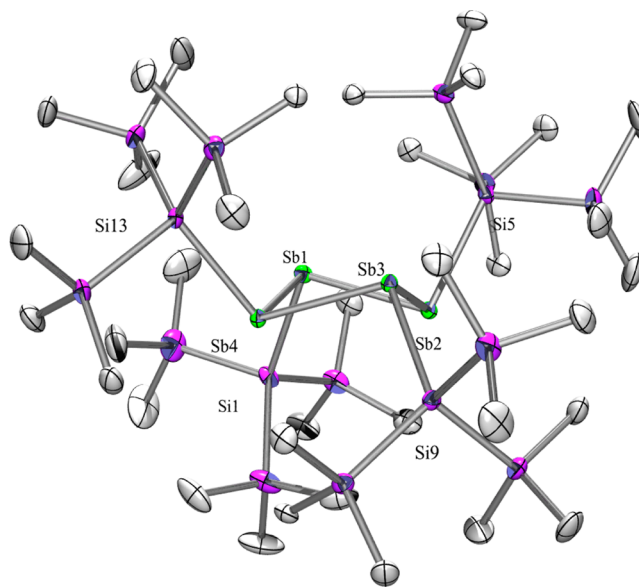


Figure 7. Molecular structure of **9** (thermal ellipsoid plot drawn at the 30% probability level). Two molecules of cocrystallizing THF are not shown. All hydrogen atoms are omitted for clarity. Bond lengths given in angstroms, angles in degrees. Sb(1)–Si(1) 2.6193(17), Sb(1)–Sb(4) 2.8530(9), Sb(1)–Sb(2) 2.8647(8), Sb(2)–Si(5) 2.6165(16), Sb(2)–Sb(3) 2.8535(9), Sb(3)–Si(9) 2.6313(16), Sb(3)–Sb(4) 2.8700(9), Sb(4)–Si(13) 2.6303(16), Si(1)–Si(2) 2.336(3), Si(2)–C(1) 1.868(8), Sb(4)–Sb(1)–Sb(2) 85.941(15), Sb(3)–Sb(2)–Sb(1) 87.450(15), Sb(2)–Sb(3)–Sb(4) 85.834(14), Si(13)–Sb(4)–Sb(1) 106.70(4), Si(13)–Sb(4)–Sb(3) 105.93(4), Sb(1)–Sb(4)–Sb(3) 87.358(15).

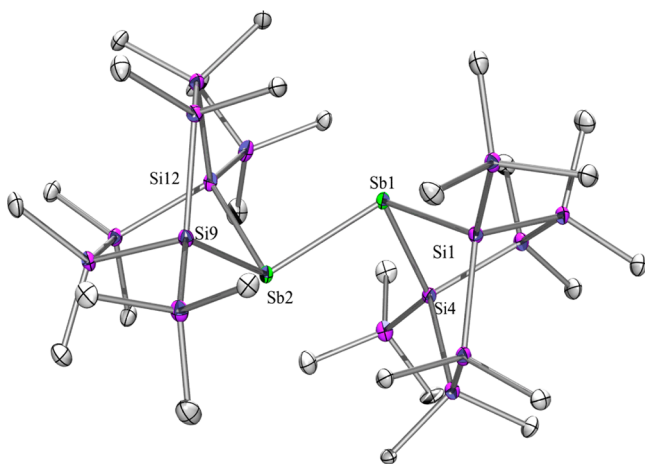


Figure 6. Molecular structure of **6** (thermal ellipsoid plot drawn at the 30% probability level). All hydrogen atoms are omitted for clarity. Bond lengths given in angstroms, angles in degrees. Sb(1)–Si(1) 2.6165(17), Sb(1)–Si(4) 2.636(2), Sb(1)–Sb(2) 2.8646(8), Sb(2)–Si(12) 2.622(2), Sb(2)–Si(9) 2.623(2), Si(1)–Si(2) 2.335(3), Si(2)–C(1) 1.891(5), Si(1)–Sb(1)–Si(4) 84.56(6), Si(12)–Sb(2)–Si(9) 85.35(6).

(EMe₃)₂ (E = Si, Ge, Sn), the distibine units of **3**, **9**, and **11** are well-separated by the large oligosilanyl parts of the molecules.

Bromostibine **4** (Figure 5) was found to crystallize in the monoclinic space group *C2/c*. The Sb–Br unit was found to be disordered over two positions, with the bromine atom being either above or below the ring plane. Cyclotetrastibine **9** was reported to crystallize in the orthorhombic space group *Pbcn*.⁷ Our crystals of **9** (Figure 7) contain THF and crystallized in the monoclinic space group *P2(1)/c*. Nevertheless, the metrical parameters observed are very similar to those reported earlier. Tris(trimethylsilyl)silylated stibine **12** (Figure 9) again shows that a larger substituent on the Sb atom causes steric interactions with the trimethylsilyl groups of the five-membered ring. To avoid these interactions, the angle of the Sb–Si(SiMe₃)₃ bond with the Si–Sb–Si plane of the ring

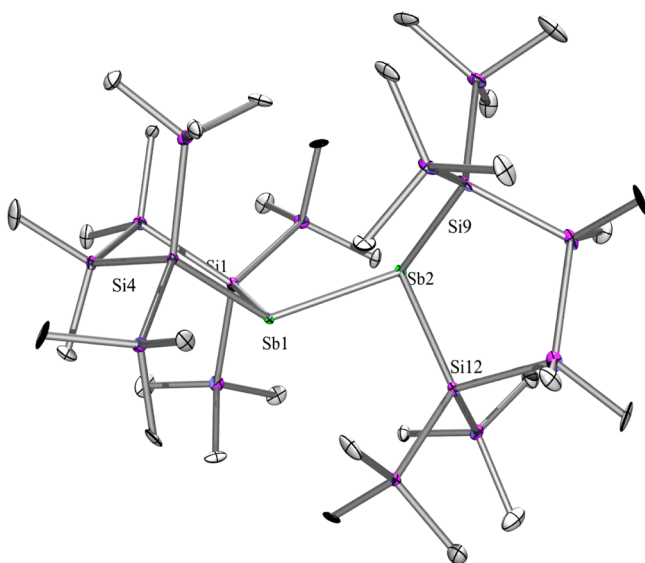


Figure 8. Molecular structure of **11** (thermal ellipsoid plot drawn at the 30% probability level). Two molecules of **11** as well as two toluene molecules are found in the asymmetric unit. Only one molecule is shown. All hydrogen atoms are omitted for clarity. Bond lengths given in angstroms, angles in degrees. Sb(1)–Si(4) 2.618(3), Sb(1)–Si(1) 2.631(3), Sb(1)–Sb(2) 2.8789(16), Sb(2)–Si(12) 2.609(3), Sb(2)–Si(9) 2.619(3), Si(1)–Si(6) 2.357(5), Si(2)–C(1) 1.872(13), Si(4)–Sb(1)–Si(1) 99.18(10), Si(4)–Sb(1)–Sb(2) 124.61(8), Si(1)–Sb(1)–Sb(2) 100.41(8), Si(12)–Sb(2)–Si(9) 99.12(11), Si(12)–Sb(2)–Sb(1) 95.41(8), Si(9)–Sb(2)–Sb(1) 127.64(8), Si(2)–Si(1)–Sb(1) 107.09(14), Si(21)–Si(17)–Sb(3) 104.69(14).

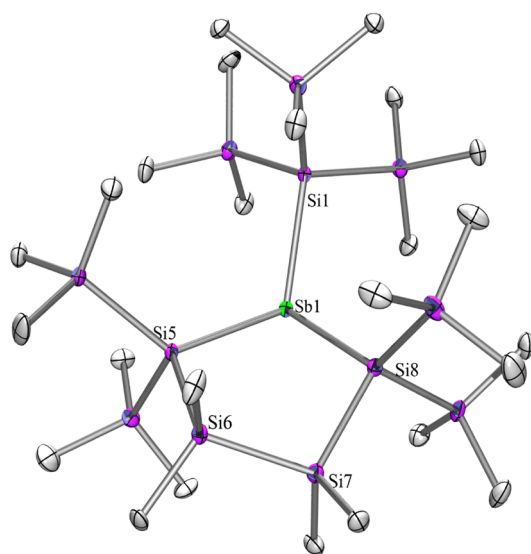


Figure 9. Molecular structure of **12** (thermal ellipsoid plot drawn at the 30% probability level). All hydrogen atoms are omitted for clarity. Bond lengths given in angstroms, angles in degrees. Sb(1)–Si(8) 2.6226(15), Sb(1)–Si(1) 2.6292(17), Sb(1)–Si(5) 2.6377(15), Si(1)–Si(2) 2.361(2), Si(2)–C(1) 1.875(7), Si(8)–Sb(1)–Si(1) 111.58(5), Si(8)–Sb(1)–Si(5) 100.43(5), Si(1)–Sb(1)–Si(5) 117.60(5).

diminished to $49.29(6)^\circ$, which is similar to that found in distibine **11**. Also, for **12**, the degree of pyramidalization is rather low, which is reflected by a sum of bond angles of $329.61(5)^\circ$ and is consistent with a lack of configurational stability. In contrast to this, alkoxystibine **13**, with the less

sterically demanding *tert*-butoxy substituent (Figure 10), exhibits an angle for the Sb–O bond of $75.62(6)^\circ$ and a sum of bond angles around Sb of $296.12(5)^\circ$.

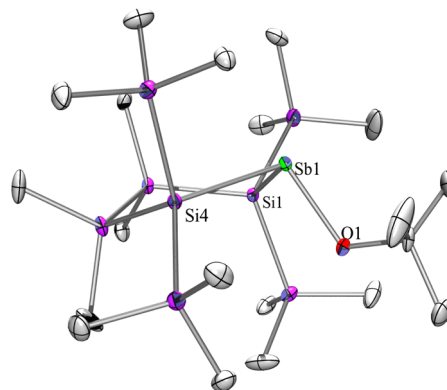


Figure 10. Molecular structure of **13** (thermal ellipsoid plot drawn at the 30% probability level). All hydrogen atoms are omitted for clarity. Bond lengths given in angstroms, angles in degrees. Sb(1)–O(1) 2.0097(17), Sb(1)–Si(1) 2.5943(8), Sb(1)–Si(4) 2.6097(10), Si(1)–Si(2) 2.3483(11), Si(2)–C(1) 1.881(3), O(1)–Sb(1)–Si(1) 96.80(6), O(1)–Sb(1)–Si(4) 101.55(5), Si(1)–Sb(1)–Si(4) 97.76(2).

2.4. Computational Study. Given the structural similarity between recently reported stibinyl radical **14**¹⁷ (Figure 11) and

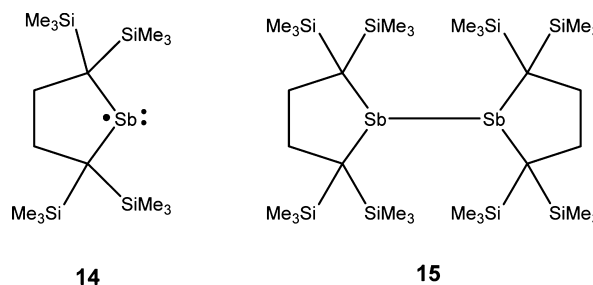
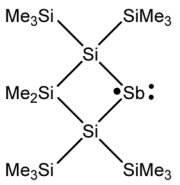
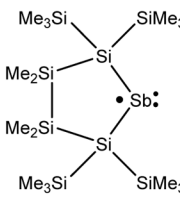


Figure 11. Recently reported stibinyl radical **14** and its dimer, **15**, formed in solid state.¹⁷

monomer of distibine **11**, the question of whether radicals are also an issue in our study led us to study computationally the dissociation processes of distibines $R_2Sb-SbR_2$ for different R substituents. The calculated dissociation energies, D_E , for distibines $Me_2Sb-SbMe_2$, $(H_3Si)_2Sb-Sb(SiH_3)_2$, and **3** are substantial and almost identical (193, 198, and 190 kJ mol^{-1} , at M06-2X/6-31G(d) (Si,C,H) SDD (Sb); see Table 3).^{8,28,29} Although D_E calculated for distibine **11** is markedly smaller ($D_E = 164 \text{ kJ mol}^{-1}$), it is still significantly higher than that predicted for the dimer, **15**, of stibinyl radical **14** ($D_E = 75 \text{ kJ mol}^{-1}$).³⁰ The high dissociation energies predicted for the Sb–Sb bonds in distibines **3** and **11** clearly rule out homolytic cleavage of the Sb–Sb bonds to a significant degree at ambient temperature. In contrast, the steric congestion brought about by the comparatively short Sb–C bonds in distibine **15** considerably weakens the Sb–Sb bond, which makes stibinyl radical formation at ambient conditions feasible in this case. The longer Sb–Si bonds in persilylated distibine **11** release part of the strain energy, which results in a stronger Sb–Sb bond. The four-membered rings in distibine **3** exert a back-pulling effect on the trimethylsilyl substituents in α position to the

Table 3. Calculated Properties of the Sb–Sb Bond in Distibines, $R_2Sb-SbR_2$, at M06-2X/SDD(Sb), Si, C, H 6-31G(d), with Experimental Data in Parentheses (See Also Supporting Information)²⁸

$R_2Sb\cdot$	D_E [kJ mol ⁻¹]	E^{rel} [kJ mol ⁻¹]	d_{Sb-Sb} [pm]	Conformer, molecular point group
$Me_2Sb\cdot^a$	193	0	288	<i>synclinal</i> , C_2
	191	2	288	<i>anticlinal</i> , C_2
	190	3	287	<i>anti-periplanar</i> , C_{2h}
$(H_3Si)_2Sb\cdot$	198	0	290	<i>synclinal</i> , C_2
	197	1	291	<i>anticlinal</i> , C_2
	195	3	291	<i>anti-periplanar</i> , C_{2h}
	190	0	290 (287.8)	<i>anti-periplanar</i> , $\theta = 180^\circ$, C_i
	172	18	291	<i>anticlinal</i> , $\theta = 155^\circ$, C_1
	124	66	291	<i>synclinal</i> , $\theta = 68^\circ$, C_1
	54	135	296	<i>syn-periplanar</i> , $\theta = 0^\circ$, C_s
	103	60	305	<i>anti-periplanar</i> , $\theta = 180^\circ$, C_i
	108	55	301	<i>anticlinal</i> , $\theta = 167^\circ$, C_1
	163	0	291 (287.7)	<i>anticlinal</i> , $\theta = 125^\circ$, C_1
	49	114	297	<i>synclinal</i> , $\theta = 28^\circ$, C_1
	-5	168	312	<i>syn-periplanar</i> , $\theta = 0^\circ$, C_s

^aExperimentally determined d_{Sb-Sb} : 281 pm (gas phase)⁴⁴ and 286.2 and 283.1 pm (solid state).^{45,46}

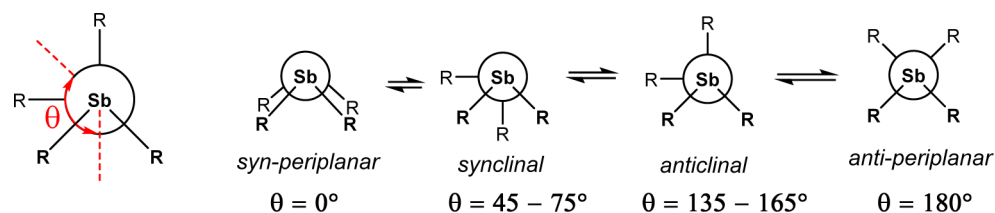


Figure 12. Conformations of distibines.

antimony atom, thereby releasing some strain imposed on the Sb–Sb linkage and leading to additional strengthening. Tetramethyldistibine, $Me_2Sb-SbMe_2$, and most of the other structurally characterized distibines, for example, distibine **3**, adopt an anti-periplanar (or simply anti) conformation (see Figure 12) around the Sb–Sb linkage in the solid state. In the gas phase, the situation for $Me_2Sb-SbMe_2$ is less clear, as both anti and clinal conformations exist at 75 °C. In this respect, it is interesting to note that sterically more congested distibines **11** and **15** adopt an unusual anticlinal conformation around the Sb–Sb bond in the solid state. A conformational analysis for tetramethyldistibine and for tetrasilyldistibine reveals a double minimum potential, with local minima for the anti-periplanar and the synclinal conformations (see Figure 12 and the Supporting Information). It is worth mentioning that for both compounds, the barriers for rotation are relatively small (13 kJ mol⁻¹ for $Me_2Sb-SbMe_2$ and 23 kJ mol⁻¹ for $(H_3Si)_2Sb-Sb(SiH_3)_2$, at MP2/def2tzvpd) and the located minima with

synclinal and anti-periplanar conformations are relatively broad. In particular, the global anti-periplanar minima are expanded to anticlinal conformations. At the density functional M06-2X/6-31G(d),SDD level, which was actually used in this study for the computations concerning experimentally observed distibines **3**, **11**, and **15**, the potential energy surface along the rotational coordinate even shows a very flat maximum for the anti-periplanar conformation (see Figure S9). The situation for heavily substituted distibines **3** and **11** is somewhat altered. The energy differences between the individual conformers are significantly more pronounced and the synperiplanar conformation of distibine **11** is actually higher in energy than for the two isolated stibinyl radicals (see Table 3). This suggests that a simple rotation process around the Sb–Sb bond in distibine **11** is not responsible for the equivalence of its trimethyl- and dimethylsilyl groups on the NMR time scale. Information regarding pyramidal inversion barriers of stibines is rather scarce. In addition to theoretical work on the inversion

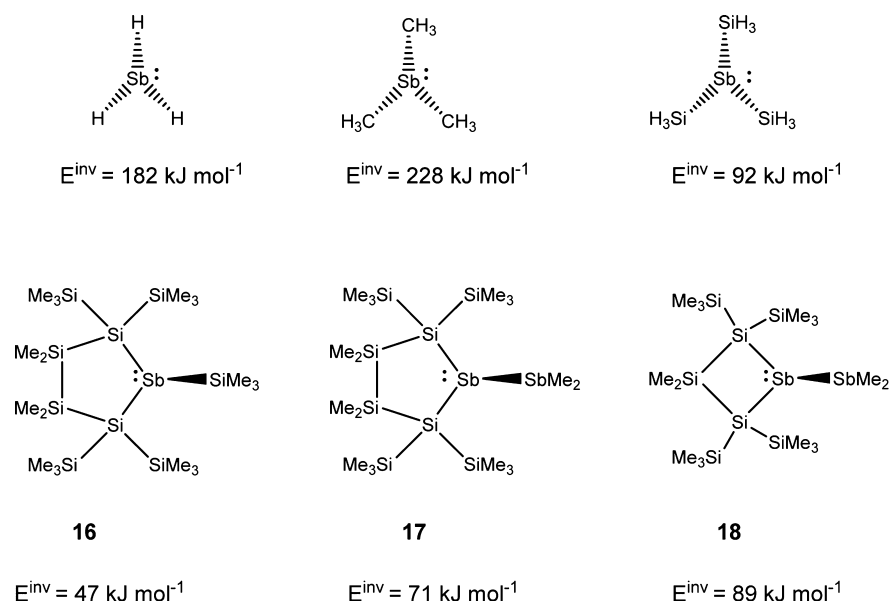


Figure 13. Calculated barriers of the pyramidal inversion of the antimony atom in stibines (at M06-2X/6-31G(d) (Si, C, H) SDD (Sb)).

of SbH_3 ^{31,32} and an early NMR study on diisopropyl-*p*-tolylstibine,³³ only a report on the isomerization of 2,3,7,8-tetramethyl-5,10-di(*p*-tolyl)-5,10-dihydrostibanthrene³⁴ is available. To get an estimate of the expected inversion barriers, E^{inv} , we investigated the inversion process of a number of model compounds such as SbH_3 , SbMe_3 , and $\text{Sb}(\text{SiH}_3)_3$ (Figure 13). The results of these calculations indicate the influence of both substituent electronegativity and sterics. Although SbH_3 and, in particular, SbMe_3 are clearly configurationally stable, the calculated inversion barrier for $\text{Sb}(\text{SiH}_3)_3$ is comparably low (92 kJ mol^{-1}) because of stabilization of the planar transition state by electrostatic and hyperconjugational effects.³⁵ Studying the pyramidal inversion processes of antimony atoms incorporated into the 1,4- and 1,3-silandiylene substituents present in **11** and **3** provides further insight. The inversion barrier calculated for the five-membered trimethylsilyl-substituted model compound **16** is as low as 47 kJ mol^{-1} . This small barrier indicates that for this compound the inversion process is expected to be fast at ambient temperature, which is consistent with ²⁹Si NMR data obtained for compound **16**²⁵ and the tris(trimethylsilyl)silyl substituted stibacyclopentasilane **12**. A closer model for distibines **3** and **11** is provided by the dimethylstibinylyl-substituted compounds **17** and **18**. Replacement of the silyl substituent by the stibinylyl group in **17** results in an increase of the barrier by 24 kJ mol^{-1} , and the less flexible four-membered ring in **18** increases the barrier to a similar extent (by 18 kJ mol^{-1}). The tendency revealed by these model calculations suggests that the observed magnetic equivalence of the silyl groups in distibine **11** is a result of fast inversion of the antimony atoms. Such processes are however less favored for distibine **3** because of the less flexible four-membered ring.

3. CONCLUSIONS

The chemistry of silylated antimony compounds is a field that has not received too much attention so far. The number of oligosilylated antimony compounds reported so far is four.^{5–7} Employing the chemistry of oligosilyl dianions developed in our group over recent years, we decided to synthesize a number stibacyclosilanes. Although the reactions of oligosilylanides with SbCl_3 indeed provided access to oligosilyl-

lated antimony compounds instead of the expected cyclic disilylated halostibines, formation of the respective distibines **3** and **6** was observed for the cases of magnesium 1,3-disilane **1b** and cyclic magnesium 1,4-disilane **5**. Reaction of SbCl_3 with magnesium 1,4-disilane **2b**, however, provided cyclic bromostibine **4**. The reason for this different reaction behavior is likely a better steric shielding of the antimony atom of **4**. This assumption is supported by the different conformational properties of distibine **11**, which could be formed by reductive coupling of bromostibine **4** with C_8K . Although for distibines **3** and **6** the Sb–Sb bond exhibits the typical conformational behavior of distibines, the two five-membered rings of **11** are strongly twisted. The steric interactions causing this twist are similar to what was observed recently by Iwamoto and co-workers for their solid-state dimer of a stibinylyl radical.¹⁷ Despite the structural similarity of Iwamoto's distibine and compound **11**, no radical formation can be expected by disassociation of **11**. This can clearly be deduced from a computational evaluation of Sb–Sb bond energies. Compared to short Sb–C bonds, the longer Si–Sb distances of **11** diminish the steric strain between the two five-membered rings, which is mainly responsible for an easy stibinylyl radical formation. Theoretical studies also explain the difference between distibines **3** and **6**, both of which exhibit configurational stability of antimony, and **11**, which is lacking this configurational stability.

4. EXPERIMENTAL SECTION

4.1. General Remarks. All reactions involving air-sensitive compounds were carried out under an atmosphere of dry nitrogen or argon using either Schlenk techniques or a glovebox. All solvents were dried using a column-based solvent purification system.³⁶ C_8K ³⁷ as well as compounds **2a,b**,¹³ **5**,^{13,18} and **8**^{13,38} were prepared according to published procedures. All other chemicals were obtained from different suppliers and used without further purification.

¹H (300 MHz), ¹³C (75.4 MHz), and ²⁹Si (59.3 MHz), NMR spectra were recorded on a Varian INOVA 300 spectrometer. If not noted otherwise, for all samples benzene-*d*₆ was used or, in the case of reaction samples, they were

measured with a H₂O-*d*₂ capillary in order to provide an external lock frequency signal. To compensate for the low isotopic abundance of ²⁹Si, the INEPT pulse sequence was used for the amplification of the signal.^{39,40} Elementary analysis was carried out using a Heraeus VARIO ELEMENTAR. UV–vis spectra were measured on a PerkinElmer Lambda 35 spectrometer using spectroscopy-grade pentane as solvent. The diffuse reflectance spectrum of compound **11** in the UV–vis–NIR range was obtained using a PerkinElmer Lambda 950 spectrometer equipped with an integrating Spectralon sphere and an R950 photomultiplier for the UV–vis and an InGaAs detector for the NIR range. The solid crystalline sample was transferred to the sample holder in a glovebox and then quickly measured under ambient atmosphere. Several scans were made in succession to make sure that the sensitive sample had not decomposed during the time of measurement. IR spectra were obtained using a Bruker Alpha P FT-IR-spectrometer with ATR module. Raman spectra were obtained using a PerkinElmer RamanStation 400F instrument with the solid sample in a sealed capillary under nitrogen atmosphere.

4.2. X-ray Structure Determination. For X-ray structure analyses, the crystals were mounted onto the tip of glass fibers, and data collection was performed with a BRUKER-AXS SMART APEX CCD diffractometer using graphite-monochromated Mo K_α radiation (0.71073 Å). The data were reduced to F²_o and corrected for absorption effects with SAINT⁴¹ and SADABS,⁴² respectively. The structures were solved by direct methods and refined by full-matrix least-squares method (SHELXL97).⁴³ If not noted otherwise, all non-hydrogen atoms were refined with anisotropic displacement parameters. All hydrogen atoms were located in calculated positions to correspond to standard bond lengths and angles. Crystallographic data (excluding structure factors) for the structures of compounds **3**, **4**, **6**, **9**, and **11–13** reported in this paper have been deposited with the Cambridge Crystallographic Data Center as CCDC-1008595 (**3**), -1008596 (**4**), -1008598 (**6**), -1008597 (**9**), -1008599 (**11**), -1010065 (**12**), and -1008600 (**13**). Data can be obtained free of charge at <http://www.ccdc.cam.ac.uk/products/csd/request/>.

4.3. 1,1'-Bis(2,2,4,4-tetrakis(trimethylsilyl)-1-stibadi-methylcyclopentasilanyl) (3). To a solution of SbCl₃ (72 mg, 0.361 mmol) in DME (5 mL), freshly prepared **1b** (0.361 mmol in 5 mL DME) was added dropwise at -37 °C. The solution became deep red, and a black precipitate occurred. After 12 h, the reaction was complete (controlled by means of NMR spectroscopy), and the solvent was completely removed. The remainder was treated with pentane three times and filtered over Celite. Red crystalline **3** (54 mg, 28%) was obtained by crystallization from toluene at -37 °C. Mp: 274–276 °C. ¹H NMR (δ ppm): 0.56 (s, 6H, SiMe₂), 0.52 (s, 6H, SiMe₂), 0.45 (s, 36H, SiMe₃), 0.41 (s, 36H, SiMe₃). ¹³C NMR (δ ppm): 6.40 (SiMe₂), 5.06 (SiMe₂), 4.61 (SiMe₃), 2.53 (SiMe₃). ²⁹Si NMR (δ ppm): -5.0 (SiMe₃), -8.7 (SiMe₃), -11.3 (SiMe₂), -102.1 (Si_q). UV–vis: λ₁ = 240 nm, ε₁ = 4.3 × 10⁴ l mol⁻¹ cm⁻¹; λ₂ = 310 nm, ε₂ = 2.4 × 10⁴ l mol⁻¹ cm⁻¹; λ₃ = 440 nm, ε₃ = 3.9 × 10³ l mol⁻¹ cm⁻¹.

4.4. 1-Bromo-2,2,5,5-tetrakis(trimethylsilyl)-1-stibate-tramethylcyclopentasilane (4). To a suspension of MgBr₂·Et₂O (443 mg, 1.72 mmol) in THF (3 mL), **2a** (3.43 mmol, in 4 mL THF 4 mL) was added. After 3 h, the reaction was complete (controlled by means of NMR spectroscopy) and was added slowly dropwise to a solution of SbCl₃ (373 mg, 1.64 mmol), in 5 mL THF at -37 °C. After 12 h, the reaction was

complete (controlled by means of NMR spectroscopy), and the solvent was completely removed. The remainder was treated with pentane three times and filtered over Celite. Red crystalline **4** (779 mg, 71%) was obtained by crystallization from pentane at -37 °C. Mp: 130–132 °C. ¹H NMR (δ ppm): 0.42 (s, 24H, SiMe₃ + SiMe₂), 0.26 (s, 6H, SiMe₂), 0.21 (s, 18H, SiMe₃). ¹³C NMR (δ ppm): 3.75 (SiMe₃), 2.62 (SiMe₃), -1.31 (SiMe₂). ²⁹Si NMR (δ ppm): 0.0 (SiMe₃), -7.5 (SiMe₃), -13.7 (SiMe₂), -98.1 (Si_q). Anal. Calcd for C₁₆H₄₈BrSbSi₈ 666.90: C: 28.82, H: 7.25. Found: C: 28.93, H: 7.37. UV–vis: λ₁ = 257 nm, ε₁ = 2.4 × 10⁴ l mol⁻¹ cm⁻¹; λ₂ = 284 nm (shoulder), ε₂ = 1.6 × 10⁴ l mol⁻¹ cm⁻¹.

4.5. 7,7'-Bis(1,4-bis(trimethylsilyl)-7-stibaoctamethyl-[2.2.1]bicycloheptasilanyl) (6). The procedure that was followed for **3** was used, but at room temperature in toluene using SbCl₃ (98 mg, 0.430 mmol) and **5** (0.430 mmol). Orange needles of **6** (133 mg, 56%) were obtained after crystallization from toluene at -37 °C. Mp: 218–219 °C. ¹H NMR (δ ppm): 0.51 (s, 12H, SiMe₂), 0.46 (s, 36H, SiMe₃), 0.36 (s, 24H, SiMe₂), 0.31 (s, 12H, SiMe₂). ¹³C NMR (δ ppm): 3.84 (SiMe₃), 0.10 (SiMe₂), -0.21 (SiMe₂), -1.58 (SiMe₂), -1.64 (SiMe₂). ²⁹Si NMR (δ ppm): -4.7 (SiMe₃), -26.3 (SiMe₂), -32.9 (SiMe₂), -92.8 (Si_q). Anal. Calcd for C₂₈H₈₄Sb₂Si₁₆ 1113.85: C: 30.19, H: 7.60. Found: C: 30.80, H: 7.74. UV–vis: λ₁ = 235 nm, ε₁ = 2.5 × 10⁴ l mol⁻¹ cm⁻¹; λ₂ = 265 nm (shoulder), ε₂ = 1.3 × 10⁴ l mol⁻¹ cm⁻¹; λ₃ = 430 nm, ε₃ = 1.7 × 10³ l mol⁻¹ cm⁻¹.

4.6. Tetrakis[tris(trimethylsilyl)silyl]cyclo-tetrastibine (9). The procedure that was followed for **3** was used, except for using SbCl₃ (118 mg, 0.519 mmol) and **8** (0.779 mmol) in THF. To remove the side products, the residue was subjected to sublimation. The remaining red oil was crystallized at -37 °C from pentane/Et₂O, affording deep red crystalline **9** (97 mg, 13%). ¹H NMR (δ ppm): 0.44 (s, 108H, SiMe₃). ¹³C NMR (δ ppm): 4.3 (SiMe₃). ²⁹Si NMR (δ ppm): -6.1 (SiMe₃), -114.5 (Si_q).

In the reaction of **8** with an equimolar amount of SbCl₃, bis[tris(trimethylsilyl)silyl]antimony bromide (**10**) [¹H NMR (δ ppm): 0.34 (s, 54H, SiMe₃). ²⁹Si NMR (δ ppm): -5.0 (SiMe₃), -97.5 (Si_q)] was detected spectroscopically by NMR in addition to (Me₃Si)₄Si, (Me₃Si)₃SiCl, and (Me₃Si)₃SiBr.

4.7. 1,1'-Bis(2,2,5,5-tetrakis(trimethylsilyl)-1-stibate-tramethylcyclopentasilanyl) (11). To a solution of **4** (200 mg, 0.30 mmol) in THF (2 mL), a suspension of C₈K (41 mg, 0.30 mmol) in 3 mL THF was slowly added at -37 °C. After 5 h, the reaction was complete (controlled by means of NMR spectroscopy), and the solvent was completely removed. The remainder was treated with pentane three times and filtered over Celite. Dark purple crystalline **11** (137 mg, 78%) was obtained by crystallization from toluene at -37 °C after 48 h. Mp: 131–133 °C. ¹H NMR (δ ppm): 0.43 (s, 72H, SiMe₃), 0.37 (s, 24H, SiMe₂). ¹³C NMR (δ ppm): 4.29 (SiMe₃), -1.42 (SiMe₂). ²⁹Si NMR (δ ppm): -6.5 (SiMe₃), -22.3 (SiMe₂), -112.1 (Si_q). Anal. Calcd for C₃₂H₉₆Sb₂Si₁₆ 1173.99: C: 32.74, H: 8.24. Found: C: 33.39, H: 7.58. UV–vis: λ₁ = 245 nm (shoulder), ε₁ = 5.8 × 10⁴ l mol⁻¹ cm⁻¹; λ₂ = 306 nm, ε₂ = 2.6 × 10⁴ l mol⁻¹ cm⁻¹; λ₃ = 478 nm, ε₃ = 4.3 × 10³ l mol⁻¹ cm⁻¹.

4.7. 2,2,5,5-Tetrakis(trimethylsilyl)-1-tris(trimethylsilyl)silyl-1-stibatetramethylcyclopentasilane (12). The procedure that was followed for **3** was used, except at room temperature in toluene/THF 1:1 using **4** (150 mg, 0.225 mmol) and **8** (0.113 mmol). Orange plates of **12** (170 mg, 90%) were obtained after crystallization from toluene at -37

°C. Mp: 217–219 °C. ¹H NMR (δ ppm): 0.40 (s, 12H, SiMe₂), 0.38 (s, 36H, SiMe₃), 0.37 (s, 27H, SiMe₃). ¹³C NMR (δ ppm): 3.75 (SiMe₃), –1.39 (SiMe₂). ²⁹Si NMR (δ ppm): –7.2 (SiMe₃), –8.3 (SiMe₃), –23.3 (SiMe₂), –110.8 (Si_q), –117.5 (Si_q). ¹H NMR (δ ppm, d⁸-toluene, –30 °C): 0.37 (s, 12H, SiMe₂), 0.35 (s, 36H, SiMe₃), 0.33 (s, 27H, SiMe₃). ¹³C NMR (δ ppm, d⁸-toluene, –30 °C): 3.62 (SiMe₃), 3.59 (SiMe₃), –1.48 (SiMe₂). ²⁹Si NMR (δ ppm, d⁸-toluene, –30 °C): –7.2 (SiMe₃), –8.3 (SiMe₃), –23.3 (SiMe₂), –113.3 (Si_q), –120.1 (Si_q). Anal. Calcd for C₂₅H₇₅SbSi₁₂ 843.65: C: 35.98, H: 9.06. Found: C: 34.77, H: 8.94.

4.8. 1-(tert-Butoxy)-2,2,5,5-tetrakis(trimethylsilyl)-1-stibatetramethylcyclopentasilane (13). The procedure that was followed for **3**, except for using **4** (58 mg, 0.087 mmol) in 2 mL THF and KO-tBu (10 mg, 0.087 mmol) in 2 mL THF. Reaction was complete after 6 h. Colorless crystals of **13** (53 mg, 93%) were obtained by crystallization from pentane at –37 °C. Mp: 223–225 °C. ¹H NMR (δ ppm): 1.22 (s, 9H, O-tBu), 0.44 (s, 6H, SiMe₂), 0.41 (s, 18H, SiMe₃), 0.33 (s, 18H, SiMe₃), 0.24 (s, 6H, SiMe₂). ¹³C NMR (δ ppm): 72.33 (OC(CH₃)₃), 31.22 (OC(CH₃)₃), 3.64 (SiMe₃), 2.56 (SiMe₃), –1.21 (SiMe₂), –1.38 (SiMe₂). ²⁹Si NMR (δ ppm): –3.4 (SiMe₃), –7.9 (SiMe₃), –17.8 (SiMe₂), –104.6 (Si_q). Anal. Calcd for C₂₀H₅₇OSbSi₈ (660.12): C: 36.39, H: 8.70. Found: C: 36.06, H: 8.21.

■ ASSOCIATED CONTENT

Supporting Information

Crystallographic information for compounds **3**, **4**, **6**, **9**, and **11–13** in CIF format and tables; ¹H, ¹³C, and ²⁹Si NMR spectra of compounds **3** and **9**, for which no elemental analyses were obtained, as measure of purity and additional data concerning the computational study. This material is available free of charge via the Internet at <http://pubs.acs.org>.

■ AUTHOR INFORMATION

Corresponding Authors

*E-mail: thomas.mueller@uni-oldenburg.de.

*E-mail: baumgartner@tugraz.at.

*E-mail: christoph.marschner@tugraz.at.

Notes

The authors declare no competing financial interest.

■ ACKNOWLEDGMENTS

Support for this study was provided by the Austrian Fonds zur Förderung der wissenschaftlichen Forschung (FWF) via the projects P-22678 (C.M.) and P-25124 (J.B.). The theoretical calculations were performed at the HPC Cluster HERO (High End Computing Resource Oldenburg), located at the University of Oldenburg (Germany) and funded by the DFG through its Major Research Instrumentation program (INST 184/108-1 FUGG) and the Ministry of Science and Culture (MWK) of the Lower Saxony State.

■ REFERENCES

- West, R. In *Organic Silicon Compounds Volume 1* (1989); Patai, S., Rappoport, Z., Eds.; John Wiley & Sons, Ltd.: Chichester, U.K., 2004; pp 1207–1240.
- Marschner, C. In *Functional molecular silicon compounds I*; Scheschke, D., Ed.; Springer: New York, 2014; pp 163–228.
- Marschner, C.; Baumgartner, J. In *Science of Synthesis: Houben-Weyl Methods of Molecular Transformations*; Oestreich, M., Ed.; Thieme: Stuttgart, Germany, 2013.
- Hengge, E. *Silicon Chemistry II*; Topics in Current Chemistry, Vol. 51; Springer: Berlin, Heidelberg, Germany, 1974; pp 1–127.
- Hassler, K.; Seidl, S. *J. Organomet. Chem.* **1990**, *384*, 263–270.
- Hassler, K.; Seidl, S. *J. Organomet. Chem.* **1988**, *347*, 27–31.
- Garcia, F.; Hopkins, A. D.; Kowenicki, R. A.; McPartlin, M.; Tesa, Y. *Dalton Trans.* **2004**, 2051–2052.
- Linti, G.; Köstler, W.; Pritzkow, H. *Eur. J. Inorg. Chem.* **2002**, 2643–2647.
- Marschner, C. *Organometallics* **2006**, *25*, 2110–2125.
- Markov, J.; Fischer, R.; Wagner, H.; Noormofidi, N.; Baumgartner, J.; Marschner, C. *Dalton Trans.* **2004**, 2166–2169.
- Kayser, C.; Kickelbick, G.; Marschner, C. *Angew. Chem., Int. Ed.* **2002**, *41*, 989–992.
- Fischer, R.; Frank, D.; Gaderbauer, W.; Kayser, C.; Mechtler, C.; Baumgartner, J.; Marschner, C. *Organometallics* **2003**, *22*, 3723–3731.
- Gaderbauer, W.; Zirngast, M.; Baumgartner, J.; Marschner, C.; Tilley, T. D. *Organometallics* **2006**, *25*, 2599–2606.
- Gaderbauer, W.; Balatoni, I.; Wagner, H.; Baumgartner, J.; Marschner, C. *Dalton Trans.* **2010**, 39, 1598.
- Uhl, W.; Jasper, B.; Lawerenz, A.; Marschner, C.; Fischer, J. Z. *Anorg. Allg. Chem.* **2007**, *633*, 2321–2325.
- Arp, H.; Zirngast, M.; Marschner, C.; Baumgartner, J.; Rasmussen, K.; Zark, P.; Müller, T. *Organometallics* **2012**, *31*, 4309–4319.
- Ishida, S.; Hirakawa, F.; Furukawa, K.; Yoza, K.; Iwamoto, T. *Angew. Chem.* **2014**, *126*, 11354–11358.
- Fischer, R.; Konopa, T.; Ullly, S.; Baumgartner, J.; Marschner, C. *J. Organomet. Chem.* **2003**, *685*, 79–92.
- Roller, S.; Dräger, M.; Breunig, H. J.; Ates, M.; Gülec, S. *J. Organomet. Chem.* **1989**, *378*, 327–337.
- Roller, S.; Dräger, M.; Breunig, H. J.; Ates, M.; Gülec, S. *J. Organomet. Chem.* **1987**, *329*, 319–326.
- Kuczowski, A.; Heimann, S.; Weber, A.; Schulz, S.; Bläser, D.; Wölper, C. *Organometallics* **2011**, *30*, 4730–4735.
- Bürger, H.; Eujen, R.; Becker, G.; Mundt, O.; Westerhausen, M.; Witthauer, C. *J. Mol. Struct.* **1983**, *98*, 265–276.
- Wallner, A.; Hlina, J.; Konopa, T.; Wagner, H.; Baumgartner, J.; Marschner, C.; Flörke, U. *Organometallics* **2010**, *29*, 2660–2675.
- Fischer, R.; Konopa, T.; Baumgartner, J.; Marschner, C. *Organometallics* **2004**, *23*, 1899–1907.
- Zitz, R.; Baumgartner, J.; Marschner, C. *Organometallics* **2015**, DOI: 10.1021/om501297h.
- Conquest, version 1.16 was used. Bruno, I. J.; Edgington, P. R.; Kessler, M.; Macrae, C. F.; McCabe, P.; Pearson, J.; Taylor, R. *Acta Crystallogr., Sect. B* **2002**, *58*, 389–397.
- Becker, G.; Freudenblum, H.; Witthauer, C. *Z. Anorg. Allg. Chem.* **1982**, *492*, 37–51.
- All calculations were done with the Gaussian 09 program Versions B1 and D1. Frisch, M. J.; Trucks, G. W.; Schlegel, H. B.; Scuseria, G. E.; Robb, M. A.; Cheeseman, J. R.; Scalmani, G.; Barone, V.; Mennucci, B.; Petersson, G. A.; Nakatsuji, H.; Caricato, M.; Li, X.; Hratchian, H. P.; Izmaylov, A. F.; Bloino, J.; Zheng, G.; Sonnenberg, J. L.; Hada, M.; Ehara, M.; Toyota, K.; Fukuda, R.; Hasegawa, J.; Ishida, M.; Nakajima, T.; Honda, Y.; Kitao, O.; Nakai, H.; Vreven, T.; Montgomery, J. A., Jr.; Peralta, J. E.; Ogliaro, F.; Bearpark, M.; Heyd, J. J.; Brothers, E.; Kudin, K. N.; Staroverov, V. N.; Kobayashi, R.; Normand, J.; Raghavachari, K.; Rendell, A.; Burant, J. C.; Iyengar, S. S.; Tomasi, J.; Cossi, M.; Rega, N.; Millam, J. M.; Klene, M.; Knox, J. E.; Cross, J. B.; Bakken, V.; Adamo, C.; Jaramillo, J.; Gomperts, R.; Stratmann, R. E.; Yazyev, O.; Austin, A. J.; Cammi, R.; Pomelli, C.; Ochterski, J. W.; Martin, R. L.; Morokuma, K.; Zakrzewski, V. G.; Voth, G. A.; Salvador, P.; Dannenberg, J. J.; Dapprich, S.; Daniels, A. D.; Farkas, O.; Foresman, J. B.; Ortiz, J. V.; Cioslowski, J.; Fox, D. J. *Gaussian 09*, revision D.01; Gaussian, Inc.: Wallingford, CT, 2009.
- For further details, see the Supporting Information.
- The computed enthalpy for the dissociation, ΔH^{diss} , of distibine **15** is 65 kJ mol^{–1}, which is near the experimental value, $\Delta H^{\text{diss}} = 54$ kJ mol^{–1}, reported in ref 17.
- Marynick, D. S.; Dixon, D. A. *J. Chem. Phys.* **1978**, *69*, 498–500.

- (32) Schwerdtfeger, P.; Laakkonen, L. J.; Pyykkö, P. *J. Chem. Phys.* **1992**, *96*, 6807–6819.
- (33) Jacobus, J. *J. Chem. Soc. D* **1971**, 1058–1059.
- (34) Uchiyama, Y. *Heteroat. Chem.* **2011**, *22*, 377–387.
- (35) Brook, M. A. *Silicon in organic, organometallic, and polymer chemistry*; Wiley: New York, 2000.
- (36) Pangborn, A. B.; Giardello, M. A.; Grubbs, R. H.; Rosen, R. K.; Timmers, F. J. *Organometallics* **1996**, *15*, 1518–1520.
- (37) Fürstner, A.; Weidmann, H. *J. Org. Chem.* **1989**, *54*, 2307–2311.
- (38) Farwell, J. D.; Lappert, M. F.; Marschner, C.; Strissel, C.; Tilley, T. D. *J. Organomet. Chem.* **2000**, *603*, 185–188.
- (39) Morris, G. A.; Freeman, R. *J. Am. Chem. Soc.* **1979**, *101*, 760–762.
- (40) Helmer, B. J.; West, R. *Organometallics* **1982**, *1*, 877–879.
- (41) SAINTPLUS: *Software Reference Manual*, version 6.45; Bruker-AXS: Madison, WI, 1997-2003.
- (42) Sheldrick, G. M. *SADABS*, version 2.10; Bruker-AXS: Madison, WI, 2003.
- (43) Sheldrick, G. M. *Acta Crystallogr., Sect. A* **2007**, *64*, 112–122.
- (44) Cszasz, A.; Hedberg, L.; Hedberg, K.; Ludwig, E. G.; Ashe, A. J. *Organometallics* **1986**, *5*, 2257–2259.
- (45) Ashe, A. J.; Ludwig, E. G.; Oleksyszyn, J.; Huffman, J. C. *Organometallics* **1984**, *3*, 337–338.
- (46) Mundt, O.; Riffel, H.; Becker, G.; Simon, A. *Z. Naturforsch., B* **1984**, *39*, 317–322.